J Bio Tribo Corros (2017) 3:35
DOI 10.1007/s40735-017-0095-y

Facile Synthesis of Nanosilver-Incorporated Titanium Nanotube for Antibacterial Surfaces

Sachin M. Bhosle[1,2] · **Craig R. Friedrich**[1]

Received: 18 March 2017 / Revised: 15 June 2017 / Accepted: 16 June 2017 / Published online: 21 June 2017

Abstract The battle against postoperative infection in orthopedic surgery calls for the development of surfaces with antibacterial activity on the implant side of the bacterial biofilm. Incorporation of nanosilver into titanium nanotube surfaces offers a potential solution. This study presents a novel single-step anodization approach to incorporating nanosilver particles within and among anodized titanium nanotubes on implant surfaces using a new hybrid electrolyte. The amount of nanosilver deposited on the titanium nanotubes was analyzed by varying the silver concentration in the hybrid electrolyte. Successful fabrication of titanium nanotubes by anodization of foils, rods and thermal plasma-sprayed surfaces of Ti6Al4V, and simultaneous nanosilver deposition was quantified by field emission scanning electron microscopy, transmission electron microscopy and X-ray energy-dispersive spectroscopy. Upon post-anodization heat treatment, the amorphous to anatase conversion of these structures was confirmed using X-ray diffraction analysis. This study presents a simple single-step fabrication of antibacterial titanium nanotube surfaces allowing controlled nanosilver deposition needed to avoid unintended cytotoxicity.

✉ Sachin M. Bhosle
smbhosle@mtu.edu

Craig R. Friedrich
craig@mtu.edu

[1] Multi Scale Technologies Institute, Michigan Technological University, 1400 Townsend Drive, Houghton, MI 49931, USA

[2] Vidya Pratishthan's Kamalnayan Bajaj Institute of Engineering and Technology, Baramati, India

Keywords Orthopedic · Implant infection · Antimicrobial · TiO_2 nanotube, surface anodization · Silver

1 Introduction

Lack of osseointegration and infection are among the major reasons for implant revision surgery. Despite sterilization protocols, chronic infection remains among the most serious post-arthroplasty problems. With diverse methods of antibacterial surface treatments such as germ-free surgical procedures and rigorous sterilization, bacterial infection still occurs post-surgery [1]. This may lead to complicated and expensive revision surgery requiring implant removal, increasing costs and trauma to the patient. Therefore, a clear understanding of infection pathogenesis involving microbiological interactions with the host defense system is essential [2]. Postoperative periprosthetic infections are reported to be higher than 25% [3]. There is early acute infection developed within the first 1–3 months post-surgery and chronic infection within 3–24 months [4]. The reduced immunity at the tissue–implant contact and the formation of a biofilm at the implant surface make the implant prone to infection [5]. While understanding the resistance mechanism of the biofilm to bactericidal agents, it is important to note that the penetration of a bactericidal agent cannot be opposed only by the barrier layer offered by the exopolysaccharide matrix, but there exist other mechanisms which help biofilm survival. These mechanisms of the biofilm's antibacterial resistance are due to several factors such as cell protection against antibacterial action by slow growth rate, increased cell density and late exponential growth owing to nutrient limitation, physiological changes associated with stress response, heterogeneity and location of cells within the biofilm, and phenotype induction [6]. To alleviate the biofilm

formation, the bacterial adhesion and colonization needs to be understood. Once the biofilm is formed by bacterial adhesion, it develops resistance to antibacterial treatment and host immunity response further becoming hard to remove, and is the primary cause of high rates of infection [6, 7]. Bacteria need strong early attachment with the implant surface to initiate the biofilm-associated phenotype (protection from antibiotics) and produce micro-colonies. The pathogenic matrix takes advantage of weak body immunity at the tissue–biomaterial interface. If the osteoblast cell wins the adhesion competition on the biomaterial substrate before the bacteria, then it reduces the chances of bacteria initiating the biofilm. Within this time window of opportunity, an antibacterial strategy can be utilized to discourage bacterial adhesion so that host cells can compete with bacteria for attachment [8]. Thus, a preventive approach on and below the implant surface level could be a winning strategy to target initial bacterial inhibition and increasing local immune response of the implant surface. Developing biofilm-resistant implants seems reasonable. Staphylococcal species are the most frequent and responsible bacteria with strong antibiotic resistance, contributing about 78% of implant-related infections [9]. While designing bactericidal surfaces for implants, the biocompatibility and long-term antibacterial ability are important [8].

In the context of nanoscale biological interactions, nanotexturing of implant surfaces could be a promising multifunctional approach giving enhanced osseointegration, antiinfection and bactericidal drug-eluting capabilities. The nanotexturing of long-established implant metals such as CoCrMo and titanium alloys has demonstrated enhanced osteoblast functions [10, 11] owing to similar chemical properties as that of the bulk material and the biomimetic nature of the surface with increased surface area due to nanometer-scale roughness. Specifically, anodized titanium dioxide nanotube surfaces are reported to foster osseointegration with enhanced biocompatibility compared to plain titanium surfaces [12]. The effects of the anodization conditions on the tube formation mechanism and properties for a wide range of biomedical applications have been reported in previous studies [13, 14]. Electrochemical anodization of titanium alloy in a fluoride-containing electrolyte produces ordered nanotubular surfaces. The presence of F^- ions causes oxidation and dissolution of $[TiF_6]^{2-}$ complexes leading to the formation of the tubular structure [13]. The TiNTs possess an elastic modulus of 36–43 GPa [15] which is closer to trabecular (10.4–14.8 GPa) and cortical (18.6–20.7 GPa) bone [16] representing closer mechanical properties to that of natural bone. TiNTs are demonstrated to induce growth of hydroxyapatite in simulated body fluid [17]. Improved biocompatibility of TiNTs has been reported with higher extracellular matrix formation, cell attachment due to anchoring, spreading, early differentiation and increased osteoblast proliferation [18] and increased in vivo bone formation [19]. While the nanotubes alone have been reported to show some antibacterial properties [20–23], the morphological (open volume) nature of TiNTs can be advantageous for storage, transport and delivery of drugs [24, 25] and antimicrobial agents. Thus, TiNTs attract attention as an encouraging bioactive surface modification for strong and speedy bone regeneration. The needed long-term antibacterial ability of biomaterials may be served with vertically aligned, open-porous TiNT surfaces with integrated nanosilver.

Silver (Ag) is a well-established biocidal agent which is effective against a wide range of species. Recently, the effect of silver nanoparticles is reported to induce antibacterial [26] and enhanced photocatalytic [27] ability on titanium dioxide with increased surface area. In vitro studies with silver-integrated coatings have shown long-term antibacterial effect against *Staphylococcus aureus* and *Pseudomonas aeruginosa* on fiber-reinforced composite implant surfaces [28]. The in vitro non-cytotoxicity of nano-Ag-integrated surfaces makes them a reliable antibacterial option for implants [29]. The carefully controlled loadings of silver nanoparticles (about 0.4 μg/cm^2) can kill 99.99% antibiotic-resistant bacteria and also help mammalian cell function [30]. Coatings of Ag-incorporated TiO_2 can kill bacteria (*staphylococcus aureus*) completely within 24 h along with improved surface hydrophilicity [31]. Silver-coated human implants possess high coating stability with low release of active Ag^+ ions (highest 56.4 ppb) in blood over 15 months post-surgery with no toxic side effects observed [1] whereas, silver levels of 200 ppb (<2 μg/L) in human serum are normal [32]. This builds a strong basis of belief and potential for development of nanotube implant surfaces with a controlled amount of Ag in the TiNTs to achieve improved antibacterial activity without cytotoxicity. These surfaces, capable of silver ion release, can give long-term antibacterial ability and help grow mammalian cells. In the work reported here, the integration of a controlled amount of silver into TiNTs on a variety of Ti6Al4V substrates is reported. To achieve a target amount of Ag incorporation into the TiNTs (0.4 μg/cm^2 in this work), a single-step electrochemical anodization process is described using a newly developed hybrid electrolyte that controls the silver content while ensuring desired nanotube morphology.

2 Materials and Methods

2.1 Substrate Preparation

Three types of substrates: foils, rods and thermal plasma-sprayed (TPS) alpha/beta titanium alloy (Ti6Al4V), were electrochemically anodized to fabricate nanotubes on the

surface. Alloy foils (0.5 mm thick) of ASTM B 265-11 grade 5 (TIMET, USA) were mechanically polished using #150 grit fine crocus cloth and #800 grit ultra-fine sanding cloth. After cleaning in deionized (DI) water followed by acetone, the samples were dried in air at room temperature. Coupons 10 mm × 30 mm × 0.5 mm thick were cut from the foils. Alloy rods (3 mm diameter and 30 mm long) ASTM B348 grade 5 (TIMET, USA) and TPS alloy surfaces of commercial hip stem implants were cleaned as received with no further preparation.

2.2 Design of Hybrid Electrolyte

Ethylene glycol (EG) and DI water-based electrolytes containing NH_4F are well-established recipes for fabricating nanotube morphologies on titanium substrates [33–36]. Our recent studies demonstrated the fabrication of nanotubes with inter-tubular spacing of 10–15 nm on foil (at 30 V in 4 h) and on TPS (at 60 V in 40 min) titanium surfaces with 0.2 wt.% of NH_4F [37]. This was designed to achieve well-separated nanotubular morphology favorable for osteoblast function and to keep fluorine content in the electrolyte as low as possible knowing that anodic nanotubular structures possess residual fluorine from electrolyte species [34, 38]. A hybrid electrolyte, using a combination of NH_4F and AgF (US patent 9376759) [39] yielding a specific concentration of fluorine and Ag, was used to prepare three different concentrations of silver in the electrolyte while maintaining a constant total fluoride concentration that ensures a consistent nanotube surface. This electrolyte composition design was based on the mass percent of NH_4F and AgF which results in a fluorine concentration of 103 mg/100 mL of total electrolyte from the earlier work. Because fluorine is the critical element for the nanotube formation process, its total concentration must be controlled. To provide the total fluorine mass concentration required in the electrolyte from AgF alone would result in excessive silver in the anodized surface which would be detrimental to mammal cells. Therefore, the electrolyte design first establishes a desired silver concentration, thereby setting the fluorine amount due to AgF alone. The required additional fluorine to bring the total fluorine to 103 mg/100 mL is provided by the additional NH_4F. Three combinations of AgF and NH_4F in 60 vol.% of EG and 40 vol.% of DI water are summarized in Table 1. Based on the amount of Ag, the electrolyte recipes are hereafter abbreviated as low-Ag, medium-Ag and high-Ag electrolytes.

2.3 Formation of Nanotube Surface

The nanotubes were formed by electrochemical anodization of Ti6Al4V substrates using a DC power source (Protek 3006B), with output 0–60VDC, 1.5A. The foil and rod surfaces were electrochemically anodized at 30VDC for 4 h, whereas the TPS samples were electrochemically anodized at 60VDC for 40 min, both with a graphite rod as the cathode and the Ti6Al4V as the anode, at room temperature. These times and voltages were established from the prior studies [34]. After anodization, TiNT samples were ultrasonically cleaned in DI water for 5 min and air-dried for 24 h to remove possible surface aggregation and Ag-flakes formed over the TiNTs for the higher silver concentrations during anodization. Each Ti6Al4V alloy substrate (foils, rods and TPS) was anodized with the above-described three types of electrolytes (low Ag, medium Ag and high Ag). The specific anodization conditions used for each different substrate type with resulting morphological parameters (diameter and length) are summarized in Table 2.

2.4 Surface Characterization

Characterization of the as-anodized and sonicated Ag-TiNT surfaces was performed by field emission scanning electron microscopy (FESEM, Hitachi S-4700). Relative wt.% chemical analysis was performed by energy-dispersive spectroscopy (EDS) by FESEM at 10 kV. X-ray diffraction (XRD—Scintag XDS 2000 Powder) patterns of annealed samples were taken to identify phase structures using an X-ray diffractometer having a CuKα characteristic radiation source. Diffraction patterns were collected in the range of 23–29° with a scan rate of 0.0015°/min with a step size of 0.03° and X-ray radiation of CuKα (λ − 1.540562

Table 1 Design of hybrid electrolyte

Electrolyte	Constituents added in 60% EG and 40% DI water (v/v)		Respective mass of element from each constituent			Resulting concentration of elements	
	AgF (mg/100 mL)	NH_4F (mg/100 mL)	Fluorine from AgF	Fluorine from NH_4F	Ag from AgF	Total F	Total Ag
Low Ag	20	195	2.99	100.027	17	103	17
Medium Ag	40	190	5.99	97.462	34	103	34
High Ag	200	142	29.95	73.097	170	103	170

Table 2 Morphological parameters of TiNTs

Ti6Al4V substrate	Anodization conditions	Ag concentration in Electrolyte	Average tube diameter (nm)	Average tube length (nm)
Foil	30 V–4 h	Low	120	1150
		Medium	120	1150
		High	130	1150
Rod	30 V–4 h	Low	115	1050
		Medium	125	1400
		High	135	1100
TPS	60 V–40 min	Low	35	500
		Medium	40	500
		High	65	500

A) at 45 kV and 35 mA. Transmission electron microscopy (TEM) imaging and analysis of Ag-TiNTs was performed at University of Illinois—Chicago on a JEOL-3010 TEM at an accelerating voltage of 300 kV. A single-tilt TEM holder was used. Selected HRTEM images and EDS elemental mapping data were obtained from the side and top opening of the nanotubes to examine the presence, size and chemical nature of the nanoparticles. To prepare the TEM samples, the TiO_2 nanotubes were scratched off the substrate.

2.5 Statistical Analysis

The EDS spectra were collected at four different locations on each TiNT surface for compositional characterization using standardless quantitative analysis on FESEM, and the data are reported as an average and range of those readings.

3 Results

The silver in nanoscale form, even at very low concentrations (mg/L), exhibits strong antibacterial effect, chemical reactivity and solubility [8, 40–42]. Anodization produced an Ag-incorporated TiNT layer on the surfaces. There were observable changes during anodization which were different than anodization in the electrolyte containing only NH_4F. It is hypothesized that, during anodization, the electronic charge transfer caused adsorption of Ag^+ in the electrolyte along with hydrogen bubbles evolved (as generally observed in regular NH_4F-containing electrolyte) on the graphite cathode, whereas F^- ions while moving toward the anode may have carried some Ag toward the anode. This caused a simultaneous development of nanotubes and Ag incorporation. Figure 1 shows a schematic representation of the Ag-incorporated TiNT (Ag-TiNT) formation mechanism. There is a possibility that during anodization the Ag incorporated into the TiNTs was transformed to AgO due to electrochemical oxidation in acidic environment and oxidation susceptibility of high surface energy Ag nanoparticles [36].

3.1 Morphological and Chemical Analysis

Figure 2a shows FESEM images of as-anodized Ag-TiNTs showing presence of large Ag nanoparticles sitting on the top of the nanotubes. The silver incorporation into the TiNTs is observed in two forms. There are small silver nanoparticles inside the tubes and adhering to the outside of the tube walls (medium-Ag rods in Fig. 2a). Secondly, large silver flakes (1–3 μm) are on the top of the nanotube arrays (low-Ag foil in Fig. 2a). These loosely adhering Ag nanoparticles were removed upon ultrasonic cleaning for 5 min in DI water, leaving behind tightly adhering spherical Ag nanoparticles (10–20 nm) sticking to the tube walls (high-Ag rods and TPS). This is seen in Fig. 2b which shows SEM images of morphologies representing ultrasonically cleaned TiNT surfaces. The ultrasonic cleaning removed adsorbed Ag reducing the possibility of excessive Ag^+ release in early stages after implantation. The anodization conditions and morphological parameters of TiNTs are summarized in Table 2. The nanoparticles sticking to the inner and outer walls of the nanotubes even after sonication indicate firmly attached nanoparticles. The potency of silver even at very low concentrations and

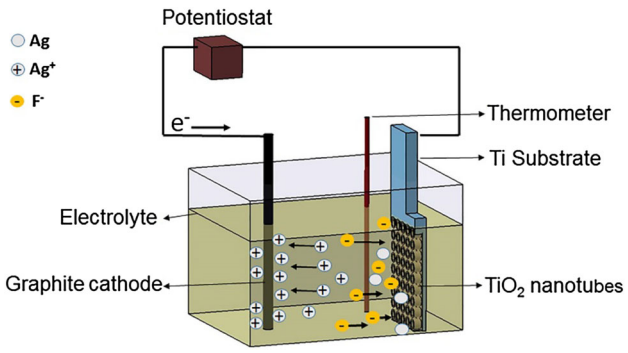

Fig. 1 Schematic representation of Ag-incorporated TiNT formation

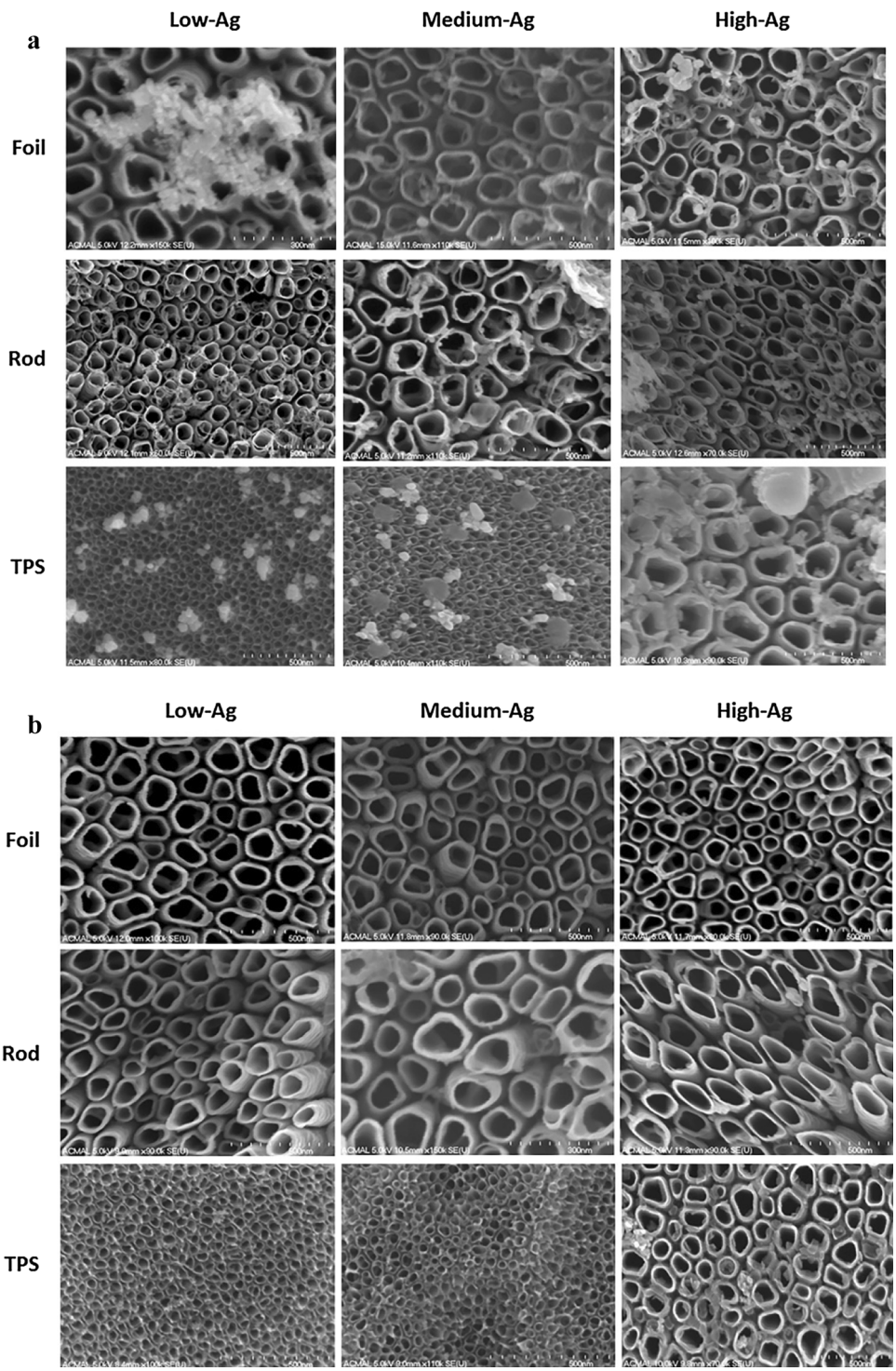

Fig. 2 **a** SEM images of as-anodized Ag-TiNT. **b** SEM images of ultrasonically cleaned Ag-TiNT

comparatively large volume availability makes Ag-TiNTs structures a potential candidate possessing long-term antibacterial abilities. This can further be improved by tailoring the amount of Ag incorporated.

The removal of loosely adherent silver accumulation from the TiNTs by sonication was reflected in the EDS analysis. Figure 3 shows a representative EDS spectrum of as-anodized and ultrasonically cleaned Ag-TiNTs. The change in the respective intensities of Ag peaks at 3 keV was observed. The Ag-TiNTs developed in the high-Ag electrolytes at the higher anodization voltage (60 V) on a relatively harder TPS substrate showed a higher amount of Ag deposition over the TiNT surfaces. The amount of Ag on and in the TiNTs showed dependence on AgF

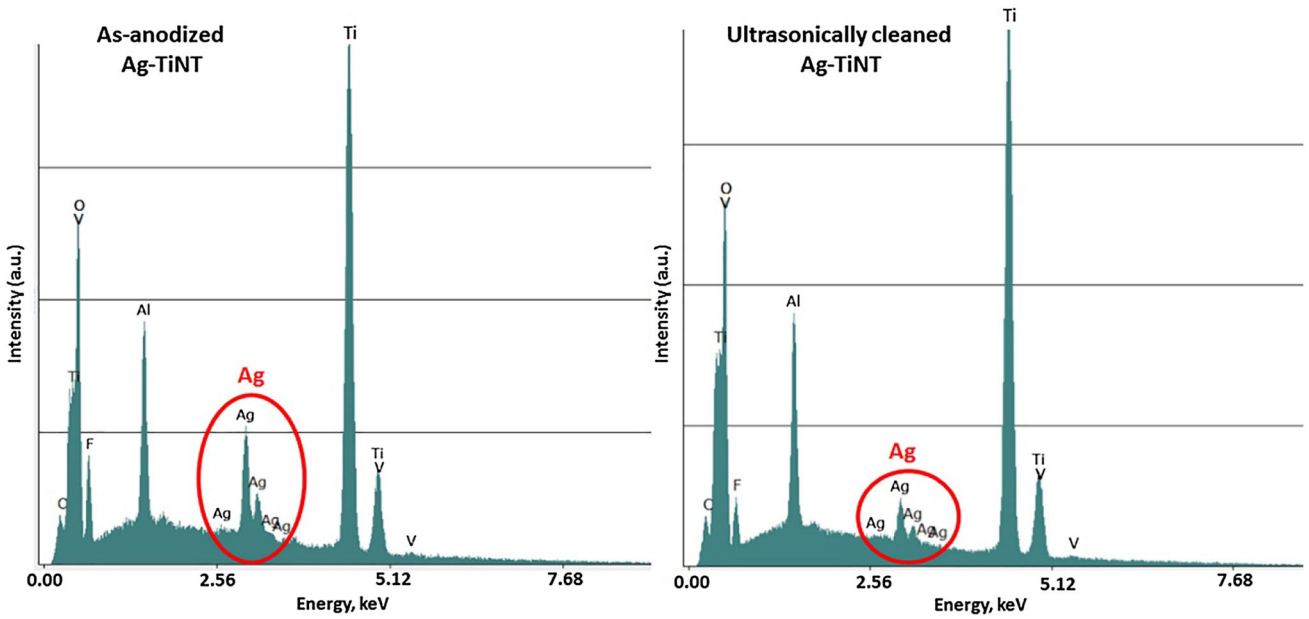

Fig. 3 Representative EDS spectra of as-anodized and ultrasonically cleaned Ag-TiNT on TPS surface

concentration in the electrolyte (low, medium and high), the type of alloy substrate (foil, rod and TPS), anodization voltage and time, and the condition of the TiNT surface (as-anodized or ultrasonically cleaned after anodizing). This was reflected in the quantitative EDS analysis. The relative wt.% variations in composition are summarized in Table 3. It should be noted that as these data are from standardless EDS, the data should be used only in relation to each other and not interpreted as an absolute surface concentration.

3.2 Estimation of Amount of Silver in Nanotube Surfaces

The volume of material removed during anodization was calculated from the area fraction and nanotube length measurements using ImageJ analysis of the FESEM images. By knowing the volume of alloy removed during the nanotube formation, and the density of TiO_2 (4.23 g/cc), the mass of the remaining nanotube layer was calculated. Based on the mass composition of Ti6Al4V alloy, the mass fraction of titanium present in the bulk alloy substrate was 90% and was used as the relative basis for the EDS relative mass percentages of the other elements. This gave the mass of titanium present in the anodized nanotubular layer. By knowing the mass of Ti present per anodized area of the nanotube structure and using the EDS wt.% ratio of Ti/Ag, the estimation of the absolute mass of silver per area (μg/cm^2) present in Ag-TiNTs was calculated.

Figure 4 shows the relationship between the Ag mass per area of the anodized TiNTs and the Ag concentration in the electrolyte. It can be clearly seen that the amount of Ag in the TiNT surface as a result of anodization depends on the Ag concentration in the electrolyte. The higher Ag concentration in the electrolyte led to a higher deposition of Ag per area over the TiNT surfaces. The data generally show a logarithmic relationship. To achieve the target concentration of 0.4 μg/cm^2 Ag on the TiNTs, these results are useful for designing the electrolyte. The results show that a wide range of Ag deposition in the TiNTs on a variety of substrates is possible. For foils, the low-Ag recipe yielded a calculated 0.46 μg/cm^2 of Ag on the as-anodized TiNT. Rods anodized in the low-Ag recipe, and upon sonication, yielded a calculated 0.31 μg/cm^2 of Ag.

Table 3 Average EDS Ag wt.% in TiNT

	Average Ag wt.% in TiNT (as-anodized)			Average Ag wt.% in TiNT (ultrasonically cleaned)		
	Foil	Rod	TPS	Foil	Rod	TPS
Low Ag	0.125	0.337	0.370	0.010	0.080	0.358
Medium Ag	0.772	0.543	1.365	0.217	0.117	0.545
High Ag	1.077	1.057	5.205	0.290	0.740	2.040

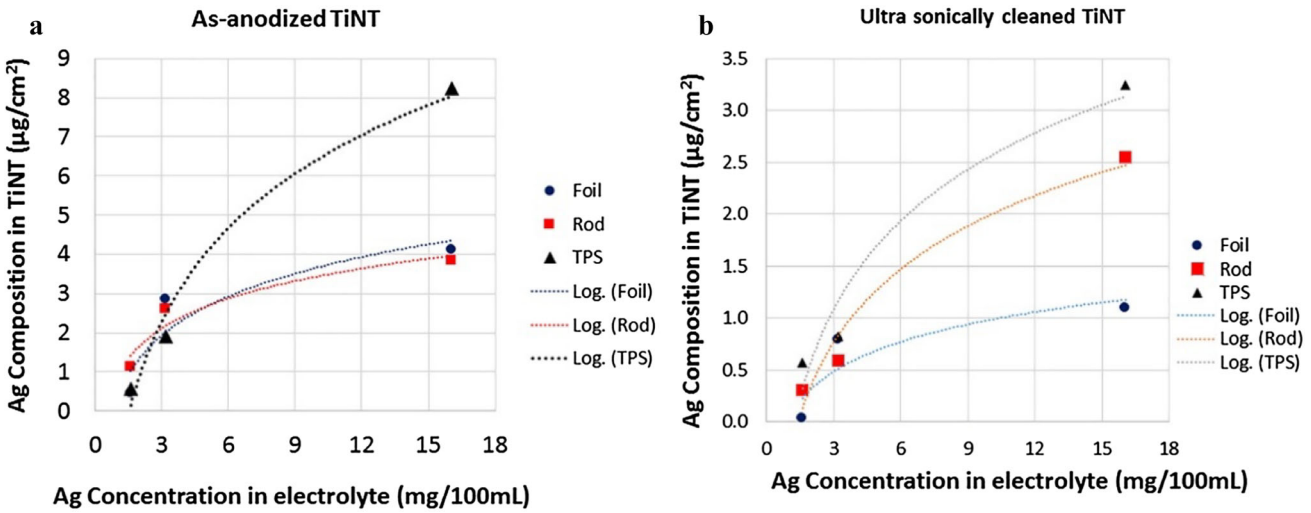

Fig. 4 Ag composition in as-anodized and sonicated Ag-TiNT surfaces with respect to Ag concentration in electrolyte

TPS substrates had higher Ag in the TiNTs compared to foils and rods. The low-Ag recipe with TPS upon sonication led to a calculated 0.57 µg/cm^2 of Ag. This may be attributed to the higher anodization voltage (60 VDC) used for TPS surfaces which created nanotubes in comparatively less time (40 min) than on foils and rods (4 h), even though the nanotubes fabricated at 60VDC were both smaller diameter and shorter than on the foils and rods. The smaller diameter nanotubes have more total surface area inside and outside the nanotubes, per lateral area, than the larger diameter nanotubes on foils and rods. This indicates that the electrolyte concentration and anodization conditions can be used to control Ag surface concentration. Such surfaces may provide resistance against infection requiring further in vivo investigations on silver ion release rate. The Ag nanoparticle-embedded titanium surfaces release Ag^+ ions and create a proton-depleted region between the bacterial membrane and the implant surface [8, 43]. The process reported provides a quick and simple method for integrating nanosilver at the implant surface level.

The surface properties of biomaterials can influence cell function in the biological environment; hence, along with morphology and chemistry, the crystallinity of the nanotube surface is another reported factor that can affect osteoblast function [44]. Heat-treated TiO_2 nanotubes of Ti and Ti6Al7Nb, with a specific anatase-to-rutile ratio, show increased hydrophilicity, enhanced bone adhesion due to high surface reactivity, increased osteoblast differentiation, gene expression and improved electrochemical stability [44]. Enhanced osteoblast adhesion and proliferation on anatase titania occurs compared to rutile and amorphous films [45]. Anatase Ag-integrated TiNTs have shown antibacterial efficacy against periodontal pathogens in vitro [46]. Figure 5 shows XRD spectra of the TiNT and Ag-TiNT foils annealed at 350 °C for 40 min. Peaks corresponding to anatase and rutile were observed on both samples. This confirmed that the presence of Ag on TiNT surface did not influence crystallinity transformation of the structure.

3.3 Silver Nanoparticle Integration: TEM Analysis

The SEM images of surface morphology show silver nanoparticles only on the surface and do not confirm the integration of silver nanoparticles within and into the nanotubes. To ensure that the nanoparticles were integrated and sticking to the tube walls are of silver, HRTEM and TEM-EDS analysis was performed. The nanotubes were scratched off the substrate and examined by TEM. Selected HRTEM images and EDS elemental mapping data were obtained from the side and top opening of the nanotubes to examine the presence, size and chemical nature of the nanoparticles.

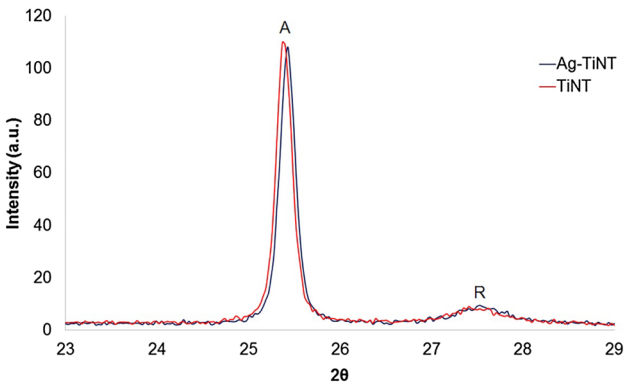

Fig. 5 XRD pattern of TiNT and Ag-TiNT annealed at 350 °C for 40 min

Figure 6 shows a HRTEM image of nanosilver spheres attached to the outside and inside walls of the nanotubes. Figure 7 shows HRTEM images, EDS layered images and elemental maps (Ti, O and Ag), which confirmed that the nanoparticles sticking to the tube walls are of silver. The HRTEM images confirmed the integration of silver nanoparticles within and into the titania nanotubes. The nanoparticles of 10–20 nm can be seen sticking to the tube walls (Figs. 6, 7a). However, few particles were little larger ($\sim$30 nm) and can be seen sticking at the top surface. Figure 8 shows the TEM-EDS spectra of corresponding elemental data for the side and top views, which further confirmed the presence of silver.

4 Discussion

To add antibacterial efficacy to TiNTs, different methods have been reported for the modification of TiNTs in recent years, utilizing high surface area and drug reserving capabilities of nanotubes. To explore the controlled local drug delivery capabilities of TiNTs and to address the problem of rapid drug release from tubes in buffered solutions having different pH, when poly lactic-co-glycolic-acid (PGLA) was added to TiNTs and tubes were loaded with carprofen and lidocaine as model drugs, swelling of TiNTs was observed to vary with pH of the surrounding buffered solutions [47]. The difficulty in maintaining in vivo pH under biological conditions may make a pH-sensitive drug delivery approach less practical. Another approach to achieving controlled drug delivery was temperature-sensitive drug delivery. Hydrogel-coated TiNTs have shown drug release in response to temperature demonstrating a potential for in vivo applications [48]. Remotely triggered therapeutics release from TiNTs using external ultrasonic input demonstrated the potential for applications in local drug delivery [49]. However, these concepts are still at a preliminary stage and need further in vivo and in vitro investigations. On the contrary, the technique such as polymethylmethacrylate bone cement loaded with metallic silver particles with a size of 5–50 nm has been reported to demonstrate high antibacterial activity and completely inhibited proliferation in vitro against *methicillin-resistant S. aureus* (MRSA), *methicillin-resistant S. epidermidis* (MRSE) and *S. epidermidis* in the absence of in vitro cytotoxicity [29]. A recent study on the modification of implant surfaces reports zirconium-incorporated TiNTs showed increased in vitro bioactivity and corrosion resistance [33]. Gold nanoparticle-integrated TiNTs formed by post-anodization magnetron sputtering leads to a heterogeneous structure [50]. Recently, zinc-incorporated [51] and copper-incorporated [52] TiNTs have been reported as alternative bactericidal agents. It is anticipated that the bacterial resistance to zinc might develop over time [53], which suggests the need of a combined approach of using multiple bactericidal agents together to address wider applicability. A TiNT surface, modified by loading Ag nanoparticles via decomposition of $AgNO_3$ by annealing (500 °C for 3 h) followed by coating with quaternary ammonium salt, showed dual action of long-term antibacterial ability and in vitro biocompatibility [54]. A similar process of Ag-TiNT formation by post-anodization immersion into $AgNO_3$ and drying in air, followed by annealing at 450 °C for 3 h and UV exposure, is another multi-step process [55]. Another process for silver deposition by post-anodization electroplating requires rinsing in acetone, isopropanol and DI water each for 5 min [36]. On the contrary, the method discussed in this study is

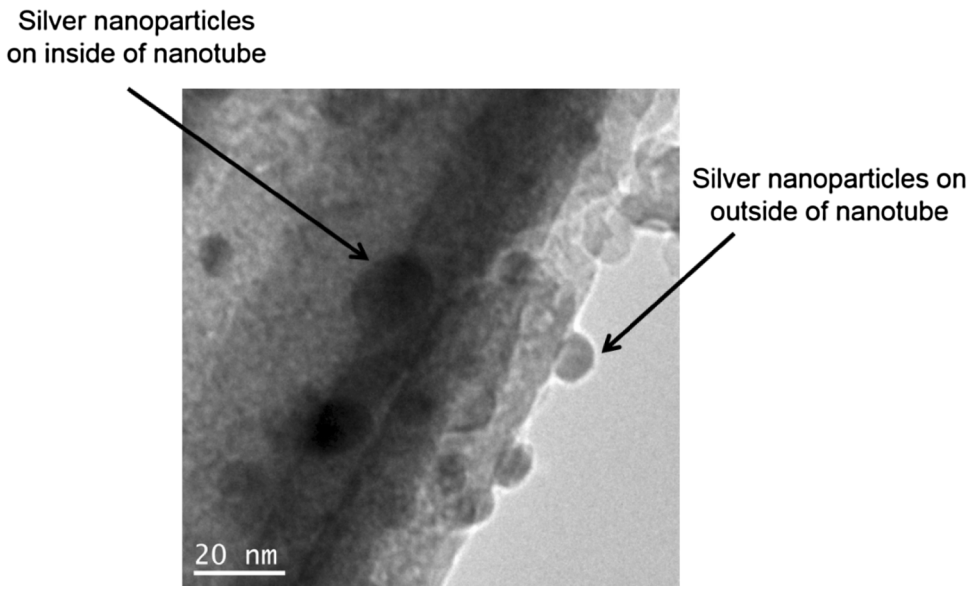

Fig. 6 HRTEM image of nanosilver spheres on inside and outside of nanotube

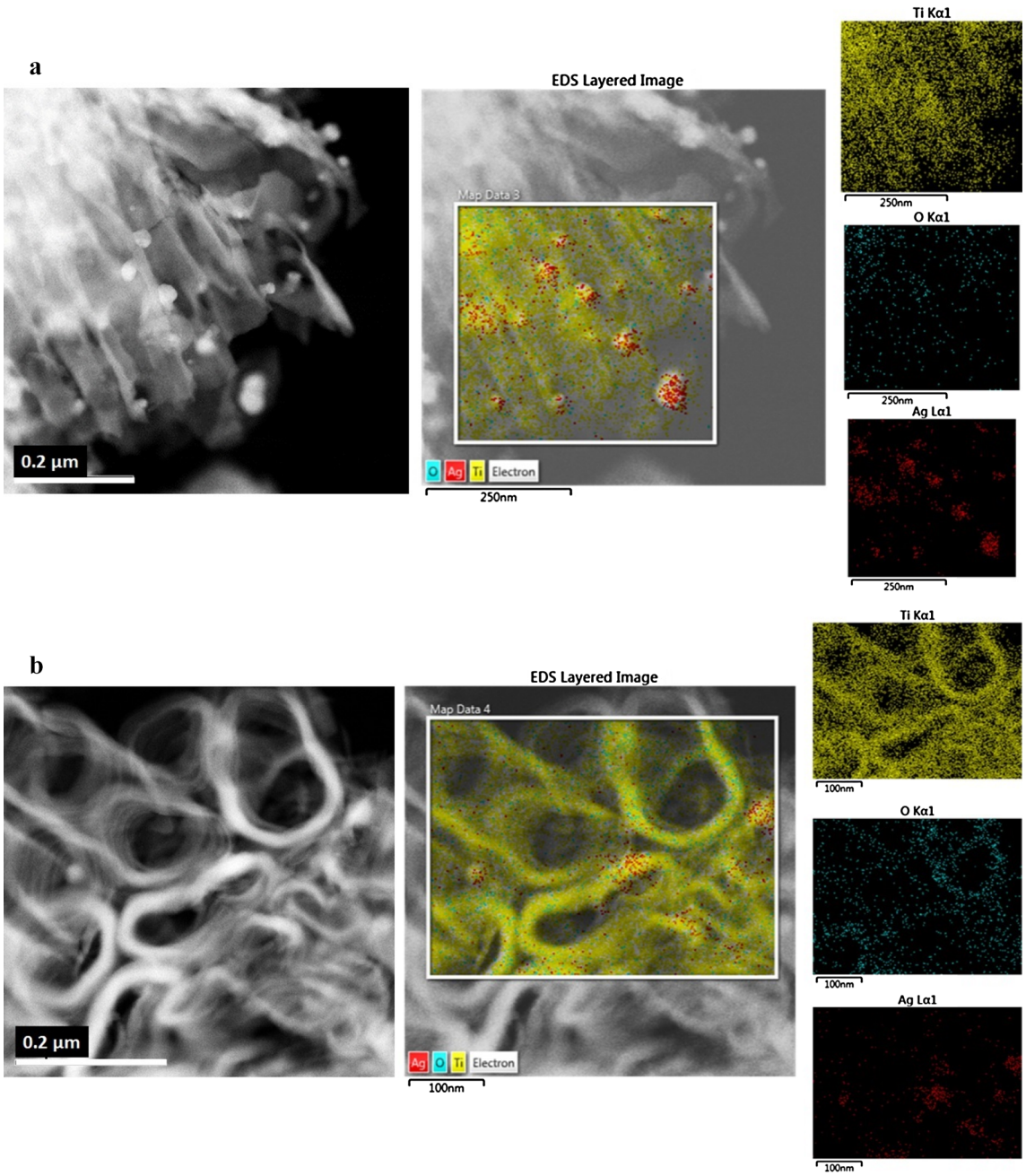

Fig. 7 HRTEM images, EDS layered images and elemental maps (Ti, O and Ag) showing Ag nanoparticles sticking to the nanotube walls. **a** *Side view* of the nanotubes and its corresponding elemental data, **b** *top view* of the nanotubes and its corresponding elemental data (courtesy Wentao Yao UI-C)

much simpler and a promising approach allowing control over the amount of Ag incorporated along with the tube morphology as any fluorine-containing electrolyte can have some fluorine contributed by AgF. This process integrates nanosilver in the same single process that forms the nanotubes, and the concentration of nanosilver in the surface can be controlled by the proper design of the new hybrid electrolyte.

5 Conclusions

The synthesis, characterization and evaluation of Ag-TiNTs, as a potential antibacterial surface, are described. A low-cost, environmentally friendly and simple yet reliable process which can give reproducible results in implant manufacturing was demonstrated. In this work, a simple single-step anodization method was demonstrated for

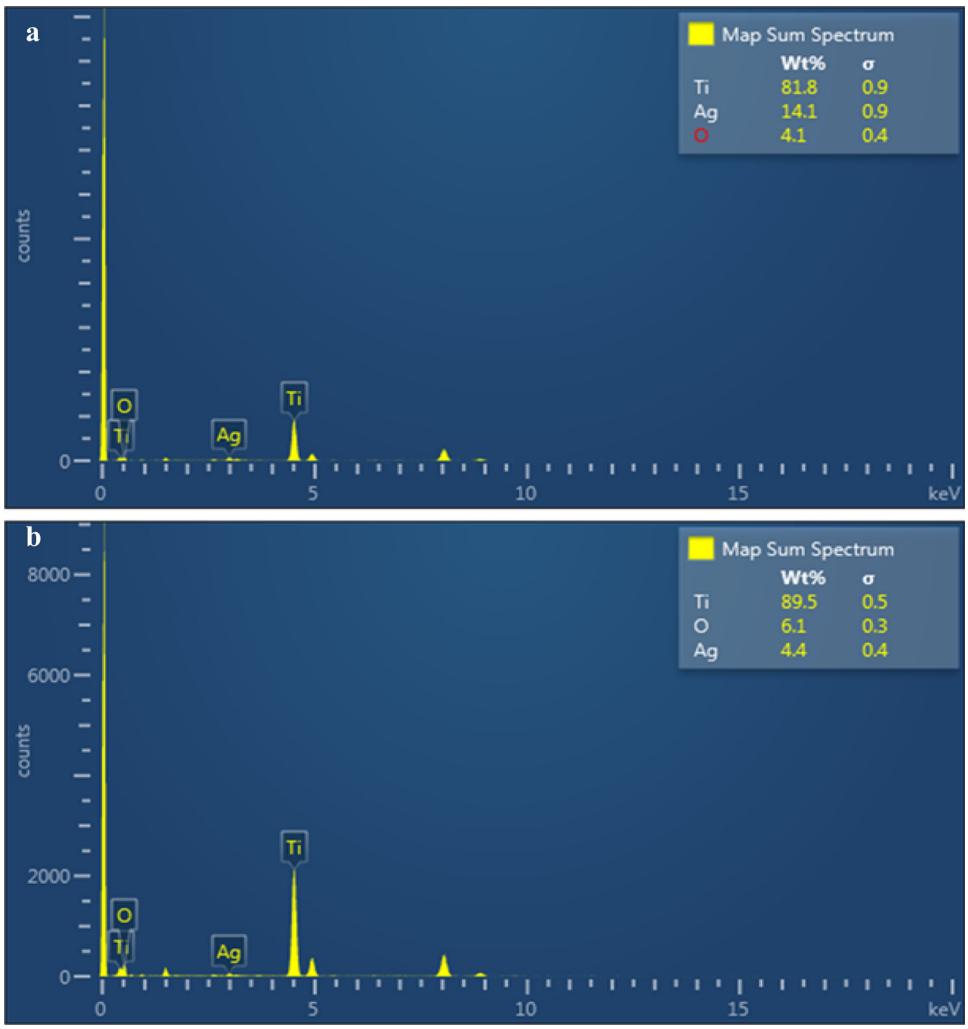

Fig. 8 The TEM-EDS spectra of corresponding elemental data for **a** side view and **b** top view (courtesy Wentao Yao UI-C)

integration of a controlled amount of nanoscale Ag over TiNT surfaces. This method offers opportunities in developing antibacterial titanium orthopedic surfaces for potentially preventing periprosthetic infection. Appropriate selection of electrolyte recipe and anodization conditions allows controlled Ag deposition on nanotubular titanium orthopedic implant surfaces to mitigate cytotoxicity. Our results retain the drug serving capacity of TiNT, which is valuable in future research in this direction. Issues related to biomechanical properties and biological interactions of such materials need further investigations in clinical settings.

Acknowledgements This work performed under the M-TRAC program was supported by Grant Case-48161 of the Twenty-First Century Jobs Trust Fund received through the Michigan Strategic Fund from the State of Michigan. The M-TRAC program is funded by the Michigan Strategic Fund with program oversight by the Michigan Economic Development Corporation. The work was also supported by the Multi-Scale Technologies Institute at Michigan Technological University.

References

1. Hardes J, Ahrens H, Gebert C, Streitbuerger A, Buerger H, Erren M et al (2007) Lack of toxicological side-effects in silver-coated megaprostheses in humans. Biomaterials 28:2869–2875
2. Song Z, Borgwardt L, Hoiby N, Wu H, Sorensen TS, Borgwardt A (2013) Prosthesis infections after orthopedic joint replacement: the possible role of bacterial biofilms. Orthop Rev 5:65–71
3. Kapadia BH, Berg RA, Daley JA, Fritz J, Bhave A, Mont MA (2016) Periprosthetic joint infection. Lancet 387:386–394
4. Zimmerli W, Trampuz A, Ochsner PE (2004) Prosthetic-joint infections. N Engl J Med 351:1645–1654
5. Zhao L, Chu PK, Zhang Y, Wu Z (2009) Antibacterial coatings on titanium implants. J Biomed Mater Res B Appl Biomater 91:470–480
6. Mah TFC, O'Toole GA (2001) Mechanisms of biofilm resistance to antimicrobial agents. Trends Microbiol 9:34–39
7. Monteiro DR, Gorup LF, Takamiya AS, Ruvollo-Filho AC, de Camargo ER, Barbosa DB (2009) The growing importance of materials that prevent microbial adhesion: antimicrobial effect of medical devices containing silver. Int J Antimicrob Agents 34:103–110

8. Gallo J, Holinka M, Moucha CS (2014) Antibacterial surface treatment for orthopaedic implants. Int J Mol Sci 15:13849–13880
9. Campoccia D, Montanaro L, Arciola CR (2006) The significance of infection related to orthopedic devices and issues of antibiotic resistance. Biomaterials 27:2331–2339
10. Webster TJ, Ejiofor JU (2004) Increased osteoblast adhesion on nanophase metals: Ti, Ti6Al4V, and CoCrMo. Biomaterials 25:4731–4739
11. Mendonca G, Mendonca DB, Aragao FJ, Cooper LF (2008) Advancing dental implant surface technology from micron to nanotopography. Biomaterials 29:3822–3835
12. Oh S, Daraio C, Chen LH, Pisanic TR, Finones RR, Jin S (2006) Significantly accelerated osteoblast cell growth on aligned TiO_2 nanotubes. J Biomed Mater Res A. 78:97–103
13. Indira K, Mudali UK, Nishimura T, Rajendran N (2015) A review on TiO_2 nanotubes: influence of anodization parameters, formation mechanism, properties, corrosion behavior, and biomedical applications. J Bio- Tribo-Corrosion 1:28
14. Indira K, Kamachi Mudali U, Rajendran N (2017) Development of self-assembled titania nanopore arrays for orthopedic applications. J Bio Tribo-Corrosion 3
15. Crawford GA, Chawla N, Das K, Bose S, Bandyopadhyay A (2007) Microstructure and deformation behavior of biocompatible TiO_2 nanotubes on titanium substrate. Acta Biomater 3:359–367
16. Rho JY, Ashman RB, Turner CH (1993) Young's modulus of trabecular and cortical bone material—ultrasonic and microtensile measurements. J Biomech 26:111–119
17. Oh SH, Finones RR, Daraio C, Chen LH, Jin S (2005) Growth of nano-scale hydroxyapatite using chemically treated titanium oxide nanotubes. Biomaterials 26:4938–4943
18. Das K, Bose S, Bandyopadhyay A (2009) TiO_2 nanotubes on Ti: influence of nanoscale morphology on bone cell-materials interaction. J Biomed Mater Res A 90:225–237
19. Vara A, Baker EA, Salisbury M, Fleischer M, Bhosle SM, Friedrich C et al (2016) Enhancing osseointegration of orthopaedic implants with titania nanotube surfaces. Foot Ankle Orthop 1:1
20. Ercan B, Taylor E, Alpaslan E, Webster TJ (2011) Diameter of titanium nanotubes influences anti-bacterial efficacy. Nanotechnology 22:295102–295112
21. Perez-Jorge C, Conde A, Arenas MA, Perez-Tanoira R, Matykina E, de Damborenea JJ et al (2012) In vitro assessment of staphylococcus epidermidis and staphylococcus aureus adhesion on TiO_2 nanotubes on Ti-6Al-4V alloy. J Biomed Mater Res A 100:1696–1705
22. Peng Z, Ni J, Zheng K, Shen Y, Wang X, He G et al (2013) Dual effects and mechanism of TiO_2 nanotube arrays in reducing bacterial colonization and enhancing C3H10T1/2 cell adhesion. Int J Nanomed 8:3093–3105
23. Golda-Cepa M, Syrek K, Brzychczy-Wloch M, Sulka GD, Kotarba A (2016) Primary role of electron work function for evaluation of nanostructured titania implant surface against bacterial infection. Mater Sci Eng C Mater Biol Appl 66:100–105
24. Torres CC, Campos CH, Diaz C, Jimenez VA, Vidal F, Guzman L et al (2016) PAMAM-grafted TiO_2 nanotubes as novel versatile materials for drug delivery applications. Mater Sci Eng C Mater Biol Appl 65:164–171
25. Wang Q, Huang JY, Li HQ, Chen Z, Zhao AZ, Wang Y et al (2016) TiO_2 nanotube platforms for smart drug delivery: a review. Int J Nanomed 11:4819–4834
26. Abdel-Fatah WI, Gobara MM, Mustafa SFM, Ali GW, Guirguis OW (2016) Role of silver nanoparticles in imparting antimicrobial activity of titanium dioxide. Mater Lett 179:190–193
27. Sobana N, Muruganadham M, Swaminathan M (2006) Nano-Ag particles doped TiO_2 for efficient photodegradation of direct azo dyes. J Mol Catal A-Chem 258:124–132
28. Nganga S, Travan A, Marsich E, Donati I, Soderling E, Moritz N et al (2013) In vitro antimicrobial properties of silver-polysaccharide coatings on porous fiber-reinforced composites for bone implants. J Mater Sci Mater Med 24:2775–2785
29. Alt V, Bechert T, Steinrucke P, Wagener M, Seidel P, Dingeldein E et al (2004) An in vitro assessment of the antibacterial properties and cytotoxicity of nanoparticulate silver bone cement. Biomaterials 25:4383–4391
30. Agarwal A, Weis TL, Schurr MJ, Faith NG, Czuprynski CJ, McAnulty JF et al (2010) Surfaces modified with nanometer-thick silver-impregnated polymeric films that kill bacteria but support growth of mammalian cells. Biomaterials 31:680–690
31. Necula BS, Fratila-Apachitei LE, Zaat SA, Apachitei I, Duszczyk J (2009) In vitro antibacterial activity of porous TiO_2-Ag composite layers against methicillin-resistant staphylococcus aureus. Acta Biomater 5:3573–3580
32. Wan AT, Conyers RAJ, Coombs CJ, Masterton JP (1991) Determination of silver in blood urine and tissues of volunteers and burn patients. Clin Chem 37:1683–1687
33. Indira K, KamachiMudali U, Rajendran N (2014) In vitro bioactivity and corrosion resistance of Zr incorporated TiO_2 nanotube arrays for orthopaedic applications. Appl Surf Sci 316:264–275
34. Bhosle SM, Tewari R, Friedrich CR (2016) Dependence of nanotextured titanium orthopedic surfaces on electrolyte condition. J Surf Eng Mater Adv Technol 06:164–175
35. Raja KS, Gandhi T, Misra M (2007) Effect of water content of ethylene glycol as electrolyte for synthesis of ordered titania nanotubes. Electrochem Commun 9:1069–1076
36. Zhao Y, Xing Q, Janjanam J, He K, Long F, Low KB et al (2014) Facile electrochemical synthesis of antimicrobial TiO_2 nanotube arrays. Int J Nanomedicine. 9:5177–5187
37. Bhosle SM, Friedrich CR (2016) Effects of aging and thermal treatment on nanotextured titanium surfaces. ORS annual meeting, Orlando, FL, USA, March 5–8
38. Regonini D, Jaroenworaluck A, Stevens R, Bowen CR (2010) Effect of heat treatment on the properties and structure of TiO_2 nanotubes: phase composition and chemical composition. Surf Interf Anal 42:139–144
39. Friedrich CR, Shokuhfar T (2013) Compositions, methods and devices for generating nanotubes on a surface. Google Patents
40. Bondarenko O, Ivask A, Kakinen A, Kurvet I, Kahru A (2013) Particle-cell contact enhances antibacterial activity of silver nanoparticles. PLoS ONE 8:e64060
41. Panacek A, Kolar M, Vecerova R, Prucek R, Soukupova J, Krystof V et al (2009) Antifungal activity of silver nanoparticles against candida spp. Biomaterials 30:6333–6340
42. Panacek A, Kvitek L, Prucek R, Kolar M, Vecerova R, Pizurova N, Sharma VK, Nevecna T, Zboril R (2006) Silver colloid nanoparticles: synthesis, characterization and their antibacterial activity. J Phys Chem B 110:16248–16253
43. Rizzello L, Pompa PP (2014) Nanosilver-based antibacterial drugs and devices: mechanisms, methodological drawbacks, and guidelines. Chem Soc Rev 43:1501–1518
44. Mazare A, Dilea M, Ionita D, Titorencu I, Trusca V, Vasile E (2012) Changing bioperformance of TiO_2 amorphous nanotubes as an effect of inducing crystallinity. Bioelectrochemistry 87:124–131
45. He J, Zhou W, Zhou X, Zhong X, Zhang X, Wan P et al (2008) The anatase phase of nanotopography titania plays an important role on osteoblast cell morphology and proliferation. J Mater Sci Mater Med 19:3465–3472

46. Yeniyol S, He Z, Yuksel B, Boylan RJ, Urgen M, Ozdemir T et al (2014) Antibacterial activity of as-annealed TiO_2 nanotubes doped with Ag nanoparticles against periodontal pathogens. Bioinorg Chem Appl 2014:829496
47. Jia H, Kerr LL (2015) Kinetics of drug release from drug carrier of polymer/TiO_2 nanotubes composite-pH dependent study. J Appl Polym Sci 132:n/a–n/a
48. Cai K, Jiang F, Luo Z, Chen X (2010) Temperature-responsive controlled drug delivery system based on titanium nanotubes. Adv Eng Mater 12:B565–B570
49. Aw MS, Losic D (2013) Ultrasound enhanced release of therapeutics from drug-releasing implants based on titania nanotube arrays. Int J Pharm 443:154–162
50. Li J, Zhou H, Qian S, Liu Z, Feng J, Jin P et al (2014) Plasmonic gold nanoparticles modified titania nanotubes for antibacterial application. Appl Phys Lett 104:261110
51. Hu H, Zhang W, Qiao Y, Jiang X, Liu X, Ding C (2012) Antibacterial activity and increased bone marrow stem cell functions of Zn-incorporated TiO_2 coatings on titanium. Acta Biomater 8:904–915
52. Hang R, Gao A, Huang X, Wang X, Zhang X, Qin L et al (2014) Antibacterial activity and cytocompatibility of Cu-Ti-O nanotubes. J Biomed Mater Res A 102:1850–1858
53. Raphel J, Holodniy M, Goodman SB, Heilshorn SC (2016) Multifunctional coatings to simultaneously promote osseointegration and prevent infection of orthopaedic implants. Biomaterials 84:301–314
54. Chen X, Cai K, Fang J, Lai M, Li J, Hou Y et al (2013) Dual action antibacterial TiO_2 nanotubes incorporated with silver nanoparticles and coated with a quaternary ammonium salt (QAS). Surf Coat Technol 216:158–165
55. Zhao L, Wang H, Huo K, Cui L, Zhang W, Ni H et al (2011) Antibacterial nano-structured titania coating incorporated with silver nanoparticles. Biomaterials 32:5706–5716